Journal of Thermal Science Vol.26, No.1 (2017) 89–95

DOI: 10.1007/s11630-017-0914-y **Article ID: 1003-2169(2017)01-0089-07**

Stereoscopic PIV Measurements of the Flow Field in a Turbine Cascade

TIAN Yangtao, MA Hongwei, MA Rong

National Key Laboratory of Science and Technology on Aero-Engines, Collaborative Innovation Center of Advanced Aero-Engine, School of Energy & Power Engineering, Beihang University, Beijing, 100191, China

This paper presents experimental measurements of the flow field in a Low-speed Turbine Cascade using a stereoscopic particle-image velocimetry (SPIV). During the measurements, a pair of frame-straddling-based CCD cameras were configured at different sides of the laser light sheet, and appropriate tracing particles (DEHS) were employed. The measurements were conducted at the incidence angle of 0 degree and exit Reynolds number of 1.7 × 10^5 with the tip clearance 1.18% of blade chord. The tip flow features, such as the evolution and breakdown of tip leakage vortex, the horseshoe vortex, turbulence characteristics of tip leakage flow, were studied for the flow field analysis. The results showed that the tip leakage flow/vortex mainly dominate flow fields in the tip region. The tip leakage vortex performs as a concentrated vortex before its breaking down and splitting into small vortices. The highest turbulence intensity mainly occurs in the tip region along with the trajectory of tip leakage vortex, and when the vortex breaks down, the turbulence intensity reduces rapidly. Additionally, the SPIV with this configuration also shows an advantage in investigating the flow structures and mechanism inside the turbine cascade.

Keywords: Stereoscopic PIV, turbine cascade, tip leakage vortex, horseshoe vortex

Introduction

The flow structures in a turbine are three-dimensional, and highly unsteady. Therefore, many flow mechanisms are still unclear and needed to make a deep exploration depending on the improvement of measurement methods. However, the traditional methods are almost based on the point measurement, which are very difficult to obtain abundant information of flow field. Currently, Particle-image Velocimetry (PIV), a new non-contact measurement technique, is used to the flow field measurement.

In the previous investigations, the PIV has been used for the flow field measurements in turbomachines by Bryanston-Cross et al. [1] and Wernet [2]. Ni [3] performed the PIV measurements on a turbine cascade. But these are all the measurements of blade-to-blade. In order to investigate the flow structures in the hub-to-tip plane, the Stereoscopic Particle-image Velocimetry (SPIV) was employed by Lang [4] and Wernet [5]. In our group, the experimental study using SPIV was conducted in an axial compressor [6]. Some special flow structures were found.

In view of the superiorities of SPIV [6-7] and rare investigations on the turbines, the SPIV measurement was conducted on a Low-Speed Turbine Cascade. The corresponding investigations of aerodynamic performance have been done using the five-hole probe [8]. In this paper, it is aimed at the study of specific flow phenomena in the turbine passage and identifying the flow mechanism, which can contribute to the further design and the improvement of the performance of the turbines.

Received: October 2016 MA Hongwei: Professor
This project was supported by Science and Technology Foundation of State Key Laboratory (Grant No. 9140C410205130C41153). And it was also funded by the National Natural Science Foundation of China, Grant No. 51161130525 and 51136003, supported by the 111 Project, No. B07009.

Nomenclature

C	chord (mm)	β	flow angle
C_x	axial chord (mm)	w_z	vorticity
R_e	Reynolds number	**Subscripts**	
C_v	streamwise velocity coefficient	1	inlet
Greek letters		2	outlet
τ	solidity		

Experimental Apparatus and Measurement Technique

Linear Turbine Cascade (LTC)

In this investigation, the measurements were performed on a Low-Speed Wind Tunnel (LSWT) driven by a centrifugal blower in Beihang University. The experimental facility was operated using LTC with the incidence angle of 0 degree and the exit Reynolds number of 1.7×10^5 based on the blade chord. The mainstream turbulence level of inlet flow is 4%.

As for the LTC, it is composed of five turbine blades, two lateral plates and two tail boards. The turbine blades are made of aluminum and mounted to the bottom lateral plate. Fig.1 shows the overall view of LSWT. All the measurements are conducted on the third blade. The two tailboards are used to adjust the periodicity of the airflow. More detailed cascade properties are summarized in Table 1. During the experiments, all the solid surfaces of the LTC are covered with the black wallpapers except for the transparent optical glass.

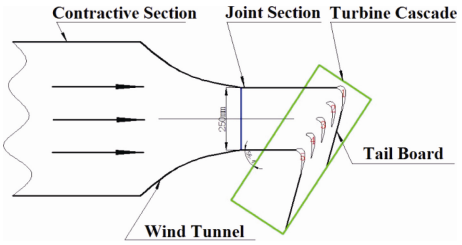

Fig. 1 Overall view of the Low-Speed Wind Tunnel (LSWT)

Table 1 Design parameters of LTC

Geometric parameters and test conditions		
Number of blades	N	5
Chord	C	102mm
Axial chord	C_x	71mm
Tip clearance	$\%C$	1.18
Solidity	τ	1.36
Inlet flow angle	β_1	33.6°
Outlet flow angle	B_2	67°
Exit Reynolds number	R_e	1.7×10^5

SPIV system and light sheet delivery

A PIV system, developed by MicroVec Incorporation, was employed in this experiment. Fig.2 presents the schematic diagram of the SPIV configuration. The laser source is a double cavity Nd: YAG laser with the maximum illumination energy of 200 mJ /pulse at a repetition rate of 15 Hz. As shown, the CCD cameras with the resolution of 2048 × 2048(4M) were configured at different sides of laser sheet with Scheimpflüg condition. The macro lens was also used. Two cameras and the laser arm were all fixed on the same mounting base which was mounted on the same three-freedom displacement mechanism.

Seeding and calibration

A uniformly high concentration of the flow seeding is the most critical element in the SPIV measurement. In this study, the flow is scattered with the oil droplets of DEHS generated by evaporating and condensing using a homemade smoke generator. The generator is capable of providing about 1 μm diameter particles. However, the oil droplet is easily condensed on the optical glass. Therefore, the optical glass of turbine cascade was designed to be removable, by which it could make the cleaning of the window quickly and thoroughly at any time.

The calibration of optical system must be performed to correct the perspective distortion caused by the inclined view of the illuminated light sheet plane and the differences in optical system magnification between the CCD cameras. The calibration target is a 50mm×50mm×6mm (length × width × thickness) black plate with 2 mm diameter calibration dots. During the calibration, nine dots arranged as the Sudoku was applied to calibrate the view. Particle analysis, image correction and grid establishment were then conducted. Finally, the 3-D calibration was automatically executed by the MicroVec software. In order to make sure that the calibration function is trustworthy, the misregistration of the two viewing directions was assessed [9-10], and the disparity map of the measurement results was illustrated in Fig.3. As shown, it can be known that the maximum displacement is 0.108743 mm which corresponds to the mismatch less than 2.7 pixels. The employment of macro lens may be one important reason for the disparity.

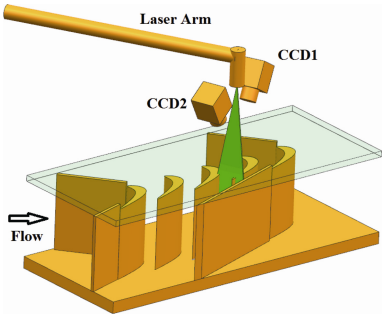

Fig. 2 Schematic diagram of the SPIV configuration

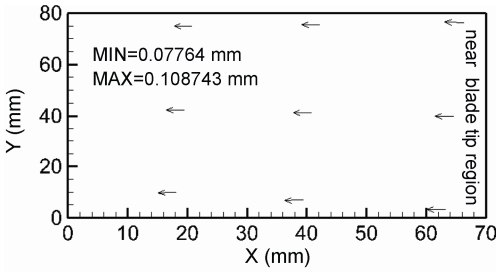

Fig. 3 Disparity map of the measurement results

Measurement layout and data processing

Fig. 4 presents the schematic layouts of the measured cross sections. The flow fields of the eight different cross sections with the interval distance of 10% blade chord between the two sections were measured.

The images were obtained inside the passage between the second blade and third blade, as can be seen in Figs. 1 and 2. In every measurement, 400 instantaneous images are acquired. The inter-frame time, dt, is set as 13 μs based on a nearly 10 m/s maximum flow velocity at inlet of LTC and yields a maximum particle-image displacement less than 8 pixels. The MicroVec V3 and in-house procedure are applied to the post-processing of SPIV. During the data processing, the interrogation window and step size are set to 32pixel × 32pixel and 12pixel × 12pixel respectively. The grid spatial resolutions of the velocity vector are about 0.039309mm. As known in references [7], the strong peak locking often appeared. In this study, some methods were employed to relieve the effect of peak locking. The histogram of the measured particle-image displacement at 50% camber line cross section, showed in Fig.5, demonstrates that the peak locking behavior is successfully controlled.

Measurement accuracy

Generally speaking, there are many factors that affect the accuracy of SPIV measurement. They usually include the random errors and bias errors which are discussed in papers [11-13]. Previous investigations show that the random errors can be minimized with attention during both the experimental investigation and data processing. In this paper, the sub-pixel fitting method applied to the MicroVec software is employed in the experiment. When the interrogation window is chosen 64pixel×64pixel, the measurement accuracy can be improved to ±0.1 pixel.

For the bias error, it is attributable to the window effect, optical setup, calibration procedure, etc. As shown in Fig. 3, the maximum displacement caused by disparity between two cameras is less than 2.7 pixels, which leads to about one tenth of the interrogation window. Based on the previous investigations, the peak locking error dominates the measurement error in instantaneous flow field, which is caused by the small particle-image diameter. It can be seen from Fig. 5 that the peak locking effect has almost been eliminated. For streamwise displacement of particle image, the accuracy is about 1.5%-4.2%. Considering that the accuracy of statistic results can be improved by ensemble-averaged, the images in every measured area need more than 300 samples.

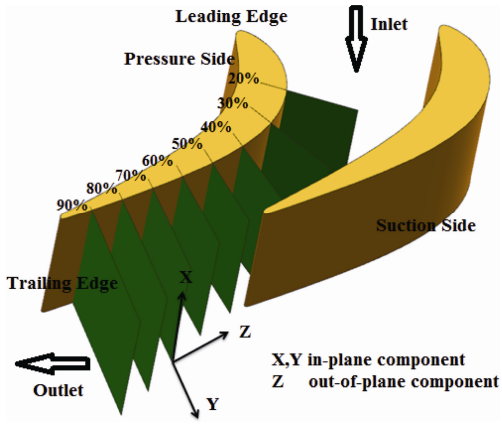

Fig. 4 Schematic layout of the measured planes

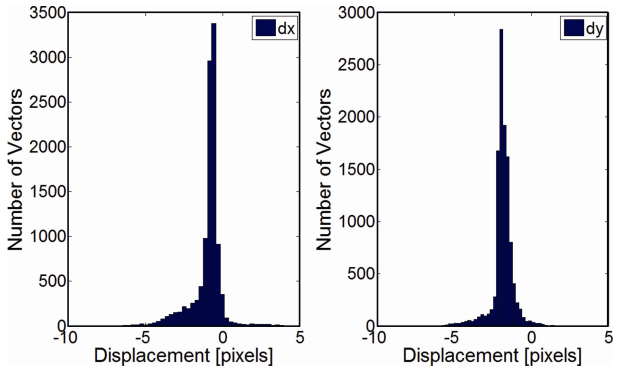

Fig. 5 Histogram of the particle-imaged displacement of dx and dy

Results and Discussions

Fig. 6 shows the instantaneous vorticity contours at 40% and 70% camber line cross section. Generally speaking, the tip leakage flow/vortex (**TLF/TLV**) mainly manifests

in the tip region above the 90% of blade height on the suction side of the blade. The TLV shows a concentrated vortex with highly positive vorticity, which the vorticity distributions being concentrated in instantaneous moment. Moreover, some small vortices with negative vorticity surround the TLV. As shown in Fig. 6(a), the TLV pattern shows irregularly, but it can still discern the vortex core. However, it shows that the TLV breaks down completely at 70% camber line cross section in Fig. 6(b). Due to the blending and diffusion as the vortex propagates downstream, the TLV which breaks into small vortices cannot present a complete vortex structure. Meanwhile, the vortex core of TLV almost disappears. It is remarkable that all the vortices are still concentrated in the middle turbine passage.

Fig. 7 lays out the instantaneous results at 50% camber line at different moments. As can be seen, the TLV is still the concentrated vortex and dominates the tip region flow. But it can be known that the morphology of TLV is always unstable. The TLV sways at every instantaneous moment, which means a strong three-dimensional, highly unsteady and transient flow in the turbine passage. Moreover, some small vortices with positive and negative vorticity always surround the core of the TLV. Simultaneously, the vorticity intensities are also changing.

Fig. 8 presents the vector contours and the streamline contours at 40% and 70% camber line. As shown in Fig.8(c), a pair of vortexes with opposite rotations is formed. The clockwise vortex rotated oppositely to the TLV appears at this cross section. But it then disappears at 70% camber line, shown in Fig. 8 (d). As known from the previous investigations, it may be the pressure-side leg of leading-edge horse-shoe vortex that has been found inside the turbine cascade [14]. The similar flow structures also appear in axial compressors [7]. Besides, the TLV intensity reduced rapidly at 70% cross section, due to fortified blending and diffusion of the TLF and mainstream. Another reason is that no more flows in the

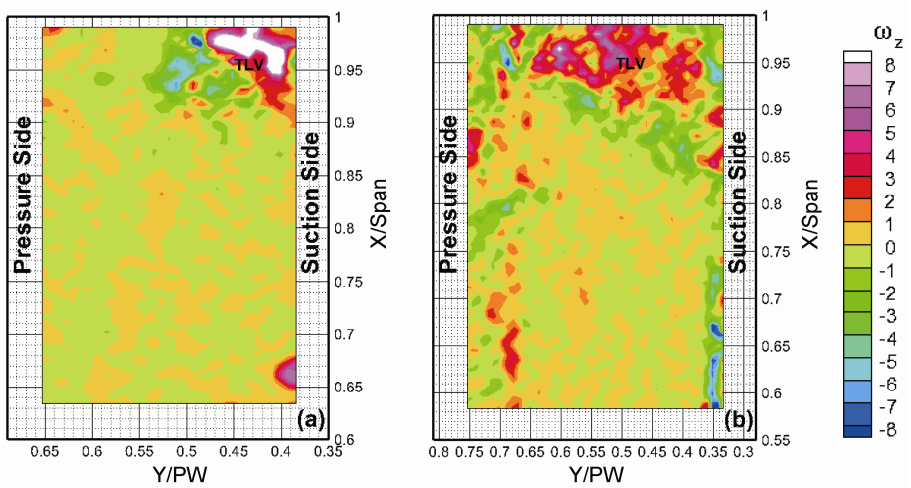

Fig. 6 Instantaneous vorticity contours at different cross sections (a) 40% (b) 70%

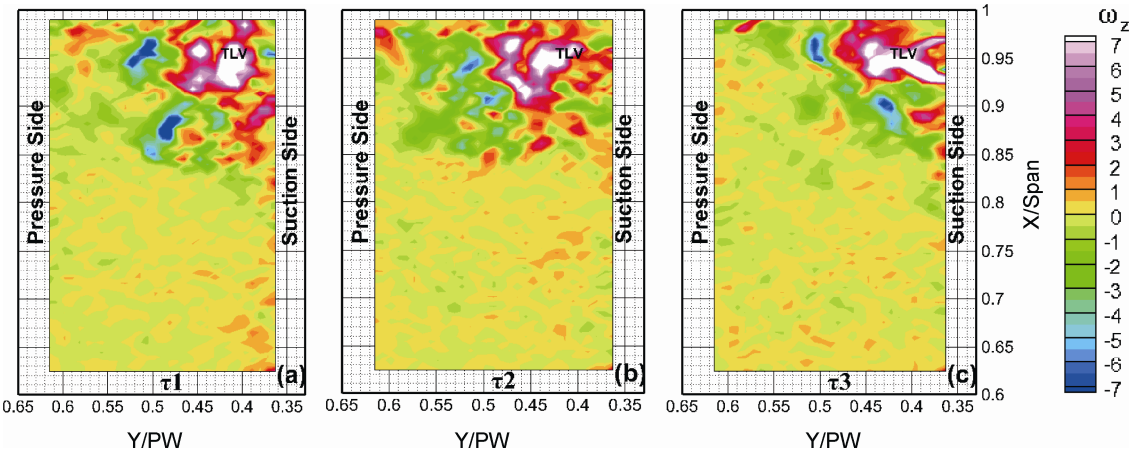

Fig. 7 Instantaneous contours at 50% camber line cross section at different moments

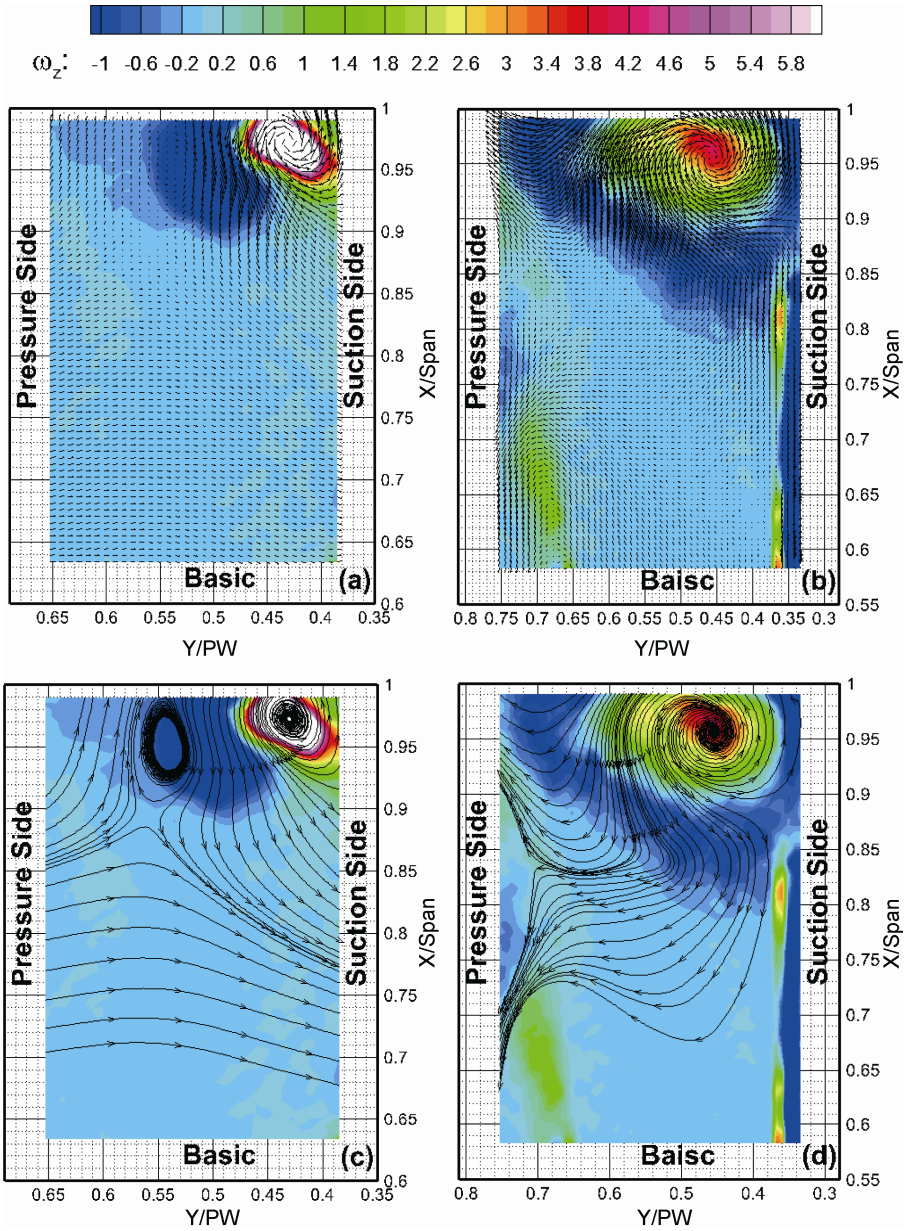

Fig. 8 Contours of vectors and streamlines at different cross sections. (a) 40% (b) 70% (c) 40% (d) 70%

pressure side are involved into the TLF, which results in the low momentum flow occupying the entire tip passage and aggravating the blockage and losses.

It is evident that lots of useful information, such as the initiation and development of the TLV, the breakdown of TLV and the horseshoe vortex, can be obtained from the ensemble-averaged result. Although the pressure gradient inside the turbine passage is favorable, the flow field still presents three-dimensional and highly unstable. The ensemble-averaged measured results from 20% to 90% camber line cross sections are shown in Fig. 9(a). The TLV appears at 30% camber line cross section with high positive vorticity. As the vortex propagates downstream, the TLV develops stronger and stronger until to 50% cross section. After this position, the TLV becomes unstable but is still a concentrated vortex, which shows an elliptical shape. After 70% cross section, the TLV breaks into the small vortices, resulting in the obvious expansion of low momentum flow in the tip region.

Until to the 90% cross section, the low momentum flow has filled into the upper semi-passage, which causes serious blockage, as shown in Fig. 9(b). Compared with the instantaneous results, the ensemble-averaged results show a low vorticity, which is because some small fluctuations are averaged.

Besides, the turbulence intensity distributions at different measured cross sections are shown as combined maps in Fig. 9(c). It is showed that the tip region has the

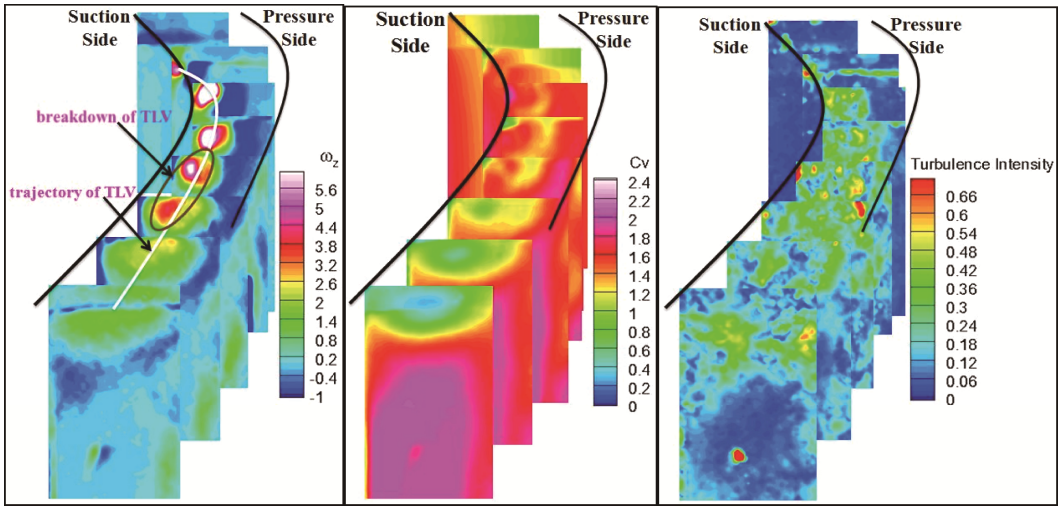

Fig. 9 Contours of vorticity, streamwise velocity and turbulence intensity at different cross sections

highest turbulence intensity along the trajectory of TLV except that it has the feeble turbulence intensity near leading edge where the TLF has not occurred. Obviously, the region with high turbulence intensity cannot be concentrated in a specific area. Compared with the vorticity map in Fig. 9(a), the turbulent flow is mainly located in the tip region near suction side. As the strengthened TLV migrates downstream, the turbulence intensity becomes large. When the TLV begins to sway and break down, the turbulent flow expands slowly to the whole passage. After that, the vortex breaks into small vortices, and the turbulence intensity reduces speedily. At this time, small vortices mix with the mainstream and dissipate gradually.

Conclusions

In this investigation, the SPIV measurements with the configuration that the CCD cameras were placed at different sides of the laser light sheet were used to investigate the flow fields inside the turbine passage. Some specific flow features inside the passage, such as the TLV evolution, TLV breakdown, and turbulence characteristics, were revealed. And it could be concluded as follows:

(1) For the instantaneous results, the morphology of vortex is always swaying and changing at every moment, which suggests the strongly three-dimensional unsteadiness of the tip flow.

(2) The TLF/TLV dominates the whole tip region flow above 90% of passage height. Before the breakdown of TLV, it mainly shows a concentrated vortex. From 60% cross section, the TLV starts to split into small vortices and the low momentum flow expands and imbues the entire tip region, resulting in the serious blockage of the tip region.

(3) At 40% camber line cross section, it can be seen that the pressure-side leg of the horse-shoe vortex with highly negative vorticity in tip region appears. As the vortex propagates downstream, it becomes hardly visible.

(4) The tip region along the trajectory of TLV shows the highest turbulence intensity. After the TLV breakdown, the turbulence intensity reduced quickly because of the mixing and the diffusion.

Acknowledgement

This project was supported by Science and Technology Foundation of State Key Laboratory (Grant No. 9140C410205130C41153). And it was also funded by the National Natural Science Foundation of China, Grant No. 51161130525 and 51136003, supported by the 111 Project, No. B07009.

References

[1] Bryanston-Cross P J, Towers C E, Judge T R, et al.: The Application of Particle Image Velocimetry (PIV) in a Short Duration Transonic Annular Turbine Cascade, ASME Transactions Journal of Turbomachinery, 114(3): 504−509, (1991).

[2] Wernet M P.: PIV for turbomachinery applications, Proceedings of SPIE - The International Society for Optical Engineering, 3172: 2−16, (1997).

[3] Ni Bing, Xu Jie, Xue Ronghai, et al.: Quantitative Measurement and Visualization of Flow around Plate Cascade Using PIV, Journal of Ship Mechanics, vol.2, (3): 1−5, (1998).

[4] Lang H, Mørck T, Woisetschläger J.: Stereoscopic Particle Image Velocimetry in a Transonic Turbine Stage, Experiments in Fluids, 32(6): 700−709, (2002).

[5] Wernet M P, Zante D V, Strazisar T J, et al.: Characteriza-

tion of the Tip Clearance Flow in an Axial Compressor Using 3-D Digital PIV, Experiments in Fluids, 39(4): 743−753, (2001).

[6] Ma, Hongwei, et al.: Experimental investigation of effects of suction-side squealer tip geometry on the flow field in a large-scale axial compressor using SPIV, Journal of Thermal Science, 24(4): 303−312, (2015).

[7] Yu X J, Liu B J.: Stereoscopic PIV Measurement of Unsteady Flows in an Axial Compressor Stage, Experimental Thermal & Fluid Science, 31(8): 1049−1060, (2007).

[8] Ma, Hongwei, and L. Wang.: Experimental study of effects of tip geometry on the flow field in a turbine cascade passage, Journal of Thermal Science, 24(1): 1−9, (2015).

[9] Willert C.: Stereoscopic Particle Image Velocimetry for Application in Wind Tunnel Flows, Meas. Sci. Technol. 8: 1465−1479, (1997).

[10] Prasad, A. K.: Stereoscopic Particle Image Velocimetry, Exp. Fluid, 29: 103−116, (2000).

[11] Westerweel J.: Fundamentals of Digital Particle Image Velocimetry, Meas Sci Technol, 8: 1379−1392, (1997).

[12] Westerweel J.: Theoretical Analysis of the Measurement Precision in Particle Image Velocimetry, Exp. Fluids Suppl, S3–S12, (2000).

[13] Boillot A, Prasad A K.: Optimization Procedure for Pulse Separation in Cross-correlation PIV. Experiments in Fluids, 21(2): 87−93, (1996).

[14] Doliglalski T.L., Smith C.R., Walker J.D.A.: Vortex Interactions with Walls, Annu. Rev. Fluid Mech. 26. 573–616, (1994).